

RESEARCH ARTICLE

Matrix ions as internal standard for high mass accuracy matrix-assisted laser desorption/ionization mass spectrometry imaging

Axel Treu  | Andreas Römpf 

Bioanalytical Sciences and Food Analysis,
University of Bayreuth, Bayreuth, Germany

Correspondence

A. Römpf, Bioanalytical Sciences and Food
Analysis, University of Bayreuth, Bayreuth,
Germany.

Email: andreas.roempf@uni-bayreuth.de

Funding information

Deutsche Forschungsgemeinschaft, Grant/
Award Number: INST 91/373-1-FUGG and
SFB 1357

Rationale: High mass accuracy is indispensable for reliable identification in matrix-assisted laser desorption/ionization mass spectrometry (MALDI MS) imaging. Ubiquitous matrix ions can serve as reference masses for mass calibration if their sum formula is known. Here we report an overview of ions generated on tissue by 11 common MALDI matrices for use in internal or external mass calibration.

Methods: Matrices covered in this study were applied onto coronal mouse brain sections using a pneumatic sprayer setup. MALDI imaging was performed on a Q Exactive HF orbital trapping mass spectrometer coupled to an AP-SMALDI 10 source. Measurements were conducted with high mass resolution (240 k full width at half maximum at m/z 200) and high mass accuracy with a root mean square mass error of better than 1.5 ppm achieved via internal mass calibration using matrix ions.

Results: MALDI MS imaging was used to investigate ions generated on tissue by 11 common MALDI matrices. An example of using matrix ions for internal mass calibration in MALDI imaging of drug substances and lipids in murine lung sections is presented. Tables containing the cluster composition, sum formulae, and the measured and theoretical m/z ratios of the identified ions were compiled for each matrix.

Conclusion: Using matrix ions as reference masses for internal and external mass calibration in MALDI MS imaging is an effective and elegant way to achieve sub-ppm mass accuracy as it makes use of ubiquitous signals present in every MALDI MS spectrum without the need for an additional calibration standard.

1 | INTRODUCTION

Mass spectrometry (MS) imaging has developed into a powerful tool for studying the distribution of analytes in tissue samples.^{1,2} Apart from desorption electrospray ionization³ and secondary ion mass spectrometry,⁴ matrix-assisted laser desorption/ionization (MALDI)¹ is the most common ionization technique used in MS imaging.⁵

In MALDI MS imaging, the sample is covered with a thin matrix layer using a variety of techniques such as pneumatic spraying or

sublimation. The matrix layer is subsequently ablated by a laser in a defined pattern.¹ This generates an array of mass spectra containing both molecular and spatial information.

The matrix used in a MALDI imaging experiment is usually a nonvolatile crystalline solid, which is able to absorb light radiation of the same wavelength as the employed laser. UV lasers are the most commonly used lasers in MALDI. For effective energy absorption and transfer onto the sample molecules, matrices used in UV-MALDI always contain a chromophore, typically electron-rich delocalized π

This is an open access article under the terms of the Creative Commons Attribution-NonCommercial-NoDerivs License, which permits use and distribution in any medium, provided the original work is properly cited, the use is non-commercial and no modifications or adaptations are made.

© 2021 The Authors. *Rapid Communications in Mass Spectrometry* published by John Wiley & Sons Ltd.

systems in the form of a central aromatic structure. Connected to this structure are substituents exerting +M or -M effects (e.g., -OH, -NH₂, -CO₂H, and -NO₂). Many common UV-MALDI matrices are derived from small aromatic organic acids such as nicotinic or phenolic acid to further assist in the formation of protonated molecules.^{6,7}

One of the major challenges in performing MS imaging of complex biological samples such as tissue sections is the identification of an analyte directly from the sample under imaging conditions. In full-scan acquisition, this is possible only with high-resolution mass spectrometry, which entails both high mass resolution and high mass accuracy. High mass resolution is required to differentiate between the multitude of superimposing isobaric peaks, whereas high mass accuracy is required to allow reliable mass identification.

The mass accuracy can be significantly improved through mass calibration. Generally, mass calibration entails the measurement of a reference or calibration compound that generates a number of known *m/z* values “reference masses” or “lock masses” that are ideally evenly distributed over a wide mass range. The theoretical *m/z* values are then matched against the actual measured values. In external mass calibration the reference compound and the actual sample are measured at different time points, whereas in internal mass calibration, the reference compound and the sample are both measured at the same time, meaning they are contained in the same spectrum.

Widely used reference compounds for external mass calibration are per- or polyfluoroalkyl substances that generate numerous equidistant ions ($\Delta m = 50, 100$ u), such as perfluorokerosene⁸ or Ultramark 1621.⁹ Furthermore, clusters of monoisotopic elements¹⁰ such as gold (Au_{*n*}⁺, Au_{*n*}⁻) or phosphorus (P_{*n*}⁺, P_{*n*}⁻) as well as clusters of monoisotopic inorganic salts¹¹ such as CsI or CsI₃ [(Cs (CsI)_{*n*})⁺, [I (CsI)_{*n*}]⁻] are widely used for external mass calibration.

In internal mass calibration, reference masses can be supplied by adding reference compounds to the sample or by ubiquitous impurities¹² such as plasticizers (e.g., phthalates) and UV stabilizers (e.g., butylated hydroxytoluene). When investigating biological samples such as thin tissue sections, well-characterized endogenous compounds (e.g., lipids) can serve as references for internal mass calibration.¹³⁻¹⁵ Matrix ions are abundant in every MALDI MS spectrum and are employed as references for internal mass calibration.^{1,15,16} Commonly used MALDI matrices such as derivatives of cinnamic acid or 2,5-dihydroxybenzoic acid (DHB) are known to form a large number of highly abundant ions,^{17,18} especially at lower mass-to-charge (*m/z*) ratios, including agglomerates with analyte ions.¹⁹ It should be noted that, in the past, this has complicated the detection and identification of “small molecules” in MALDI. This is no longer the case if high mass resolution instruments are used. On the contrary, the high number of ions in the lower mass range can be an advantage if they are used as references for internal mass calibration.

At higher *m/z* ratios, matrix ions tend to be scarcer, especially on biological tissues due to ion suppression effects^{20,21} exerted by the sample. Matrix ions found at these higher *m/z* ratios usually belong to an ascending homologous series of clusters, for example, [aDHB + NH₄-*b*H₂O]⁺.

To be usable as a lock mass in internal mass calibration, an ion is ideally detectable in the entire measurement field of view, that is on

and off sample, with sufficient abundance and should not be superimposed by neighboring signals.

In this work, we systematically investigated the ions generated on tissue by 11 common MALDI matrices (Table 1) in MS imaging experiments. Cluster compositions and sum formulae were assigned to specific matrix ions based on accurate mass measurements, and selected 2,5-DHB cluster ions were confirmed by MS/MS data. With this, we aim to provide lists of reference masses for use in internal or external mass calibration.

2 | EXPERIMENTAL

2.1 | Materials

Solvents and matrix substances were purchased from Sigma-Aldrich (Taufkirchen, Germany). Adhesive glass slides (Menzel Gläser, Superfrost) were purchased from VWR (Darmstadt, Germany). Matrices were of the highest available purity. Brains of 6 week old male and female BALB/c mice were purchased from Charles River (L'Arbresle, France). Sections of murine lung tissue for drug imaging were obtained from the surplus material of another study²² conducted in our laboratory.

2.2 | Sample preparation

Serial coronal mouse brain sections (10 μm) were cut at -25°C using a CM3050 S cryostat (Leica Microsystems, Wetzlar, Germany) and deposited onto adhesive glass slides (Menzel Gläser, Superfrost) and stored at -80°C. The sections were placed in a desiccator for 10 min before matrix application. The matrices were applied using a semiautomatic pneumatic sprayer system built in-house. The matrix solutions were prepared as follows: 1,5-diaminonaphthalene (1,5-DAN) 5 mg/mL in 50% acetone; 2,6-dihydroxyacetophenone (DHAP) and norharmane 10 mg/mL in 50% methanol; 2,5-dihydroxybenzoic acid (DHB) 30 mg/mL in 50% acetone; alpha-cyano-4-hydroxycinnamic acid (CHCA), sinapic acid (SA), and caffeic acid (CA) 10 mg/mL in 50% acetone; 9-aminoacridine (9AA) and 2[(2E)-3-(4-*tert*-butylphenyl)-2-methylprop-2-enylidene]malononitrile (DCTB) 10 mg/mL in 75% acetone; 4-nitroaniline (pNA) 5 mg/mL in 75% acetone; and 2,4,6-trihydroxyacetophenone (THAP) 15 mg/mL in 75% methanol. The matrices used in the positive ion mode were acidified with 0.1% (v/v) trifluoroacetic acid. A short overview of the matrix substances covered in this study is provided in Table 1. The structural formulae of all the matrices used in this work are given in Figure S1 (supporting information).

2.3 | MS acquisition and data analysis

MALDI MS imaging measurements were performed using a Q Exactive HF mass spectrometer (Thermo Fisher Scientific GmbH,

TABLE 1 Overview of the matrix substances covered in this study

Matrix (abbreviation)	CAS Registry Number	Sum formula	Ion mode(s)
9-Aminoacridine (9AA)	90-45-9	C ₁₃ H ₁₀ N ₂	Negative
2[(2E)-3-(4-tert-Butylphenyl)-2-methylprop-2-enylidene]malononitrile (DCTB)	300364-84-5	C ₁₇ H ₁₈ N ₂	Positive
Caffeic acid (CA)	331-39-5	C ₉ H ₈ O ₄	Positive
Alpha-cyano-4-hydroxycinnamic acid (CHCA)	28166-41-8	C ₁₀ H ₇ NO ₃	Positive
1,5-Diaminonaphthalene (1,5 DAN)	2243-62-1	C ₁₀ H ₁₀ N ₂	Negative/Positive
2,5-Dihydroxybenzoic acid (DHB)	490-79-9	C ₇ H ₆ O ₄	Positive/Negative
4-Nitronaniline (pNA)	100-01-6	C ₆ H ₆ N ₂ O ₂	Negative/Positive
Norharmane	244-63-3	C ₁₁ H ₈ N ₂	Negative/Positive
Sinapic acid (SA)	530-59-6	C ₁₁ H ₁₂ O ₅	Positive
2,4,6-Trihydroxyacetophenone (THAP)	480-66-0	C ₈ H ₈ O ₄	Negative
2,6-Dihydroxyacetophenone (2,6 DHAP)	699-83-2	C ₈ H ₈ O ₃	Positive/Negative

Bremen, Germany) coupled to an atmospheric pressure MALDI imaging source AP-SMALDI10 (TransMIT GmbH, Gießen, Germany) equipped with a $\lambda = 337$ nm N₂ laser operating at a repetition rate of 60 Hz.²³ Measurements were carried out in positive and negative ion mode with 30 laser shots per pixel and a mass resolution of 240 k (full width at half maximum) at m/z 200. The measurements intended for cluster identification were conducted using a pixel size of 30 × 30 μm covering a 20 × 20 pixel grid. These measurements employed previously identified matrix clusters for internal mass calibration, which are highlighted with an “*.” Measured m/z values given in Tables S1–S18 (supporting information) are averaged across all 400 spectra of the measurement to correct for signal fluctuation. The identification of matrix clusters was based on accurate mass identification. Theoretical masses and m/z values were calculated using tabulated values from the Commission on Isotopic Abundances and Atomic Weights²⁴ and were rounded to five decimal places. The murine lung was measured using two alternating full-scan acquisition windows from m/z 120 to 450 and m/z 700 to 900; the step size was set to 20 × 40 μm resulting in an image pixel size of 40 × 40 μm . Further information on this measurement setup can be found in our previously reported study.²²

3 | RESULTS AND DISCUSSION

For the investigation of matrix clusters, matrices were applied onto coronal mouse brain sections and measured in MALDI MS imaging. Each investigated matrix compound or compound class is presented here, starting with matrices intended primarily for use in positive ion mode. Tables containing the respective cluster composition, sum formulae, and the theoretical and measured m/z of the identified matrix clusters are provided as a basis for internal or external mass calibration.

3.1 | 2,5-Dihydroxybenzoic acid (DHB)

2,5-Dihydroxybenzoic acid or gentisic acid (DHB, C₇H₆O₄, 154.02661 u) is one of the most common matrix substances used in positive mode MALDI MS imaging for a wide range of analytes, including small molecules,²⁵ lipids,¹⁶ and peptides.²⁶ Furthermore, 2,5-DHB was shown to be suitable for the analysis of phospholipids in the negative ion mode.²⁷ In the positive ion mode, 2,5-DHB readily forms clusters based on the addition of H⁺, NH₄⁺, Na⁺, or K⁺ and subsequent dehydration. Four highly periodic cluster series of the general cluster composition $[aM + X-bH_2O]^+$ (X = H⁺, NH₄⁺, Na⁺, K⁺; $a = 1, 2, 3, \dots$; $b \leq a$) were identified, with members of the NH₄⁺ adduct $[aM + NH_4-bH_2O]^+$ series being the most abundant. An overview of this cluster series, including the cluster composition, sum formulae, and the theoretical and measured m/z , is provided in Table 2. Similar overviews of the three other DHB cluster series are provided in Tables S1–S3 (supporting information). An overview of the general composition of clusters from all matrices covered in this work is provided in Table 3. An overview of the mass spectra of DHB on mouse brain tissue is shown in Figures S2 and S3 (supporting information). In addition to these four cluster series, DHB forms a number of clusters based on hydrogen/alkali metal cation exchange followed by the loss of water. These ions share the general cluster composition $[aM + b\text{Alkali}-(b-1)H-cH_2O]^+$ ($a = 1, 2, 3, \dots$; $b = 1, 2, 3, \dots$; $c = 0, 1, 2, 3, \dots$) (Table S4 [supporting information]). A similar composition is observed for the 2,5-DHB clusters in the negative ion mode detected between m/z 150 and 850. These ions are formed based on a hydrogen/alkali metal cation exchange followed by the loss of water and share the general cluster composition $[aM-bH + (b-1)\text{Alkali}-cH_2O]^-$ ($a = 1, 2, 3, \dots$; $b = 1, 2, 3, \dots$; $c = 0, 1, 2, 3, \dots$). A number of these ions are preceded by intensive M-1 peaks caused by the loss of a hydrogen radical that has general cluster composition of $[aM-bH-H + (b-1)\text{Alkali}-cH_2O]^-$ ($a = 1, 2, 3, \dots$; $b = 1, 2, 3, \dots$; $c = 0, 1, 2, 3, \dots$) (Table S5 and

Cluster composition	Sum formula	Theoretical m/z	Measured m/z	RMSE (ppm)
M + NH ₄ -H ₂ O ⁺	C ₇ H ₈ NO ₃ ⁺	154.04987	154.04974	1.01
2M + NH ₄ -H ₂ O ⁺	C ₁₄ H ₁₄ NO ₇ ⁺	308.07648	308.07651	0.19
2M + NH ₄ -2H ₂ O ⁺	C ₁₄ H ₁₂ NO ₆ ⁺	290.06591	290.06586	0.18
*3M + NH₄-2H₂O⁺	C₂₁H₁₈NO₁₀⁺	444.09252	444.09252	-
3M + NH ₄ -3H ₂ O ⁺	C ₂₁ H ₁₆ NO ₉ ⁺	426.08196	426.08200	0.42
4M + NH₄-3H₂O⁺	C₂₈H₂₂NO₁₃⁺	580.10857	580.10840	0.40
4M + NH ₄ -4H ₂ O ⁺	C ₂₈ H ₂₀ NO ₁₂ ⁺	562.09800	562.09808	0.59
5M + NH ₄ -3H ₂ O ⁺	C ₃₅ H ₂₈ NO ₁₇ ⁺	734.13517	734.13525	0.95
*5M + NH₄-4H₂O⁺	C₃₅H₂₆NO₁₆⁺	716.12461	716.12461	-
5M + NH ₄ -5H ₂ O ⁺	C ₃₅ H ₂₄ NO ₁₅ ⁺	698.11405	698.11426	0.46
6M + NH₄-5H₂O⁺	C₄₂H₃₀NO₁₉⁺	852.14065	852.14093	0.53
6M + NH ₄ -6H ₂ O ⁺	C ₄₂ H ₂₈ NO ₁₈ ⁺	834.13009	834.12994	0.51
7M + NH₄-6H₂O⁺	C₄₉H₃₄NO₂₂⁺	988.15670	988.15729	0.54
7M + NH ₄ -7H ₂ O ⁺	C ₄₉ H ₃₂ NO ₂₁ ⁺	970.14613	970.14697	0.71
*8M + NH₄-7H₂O⁺	C₅₆H₃₈NO₂₅⁺	1124.17274	1124.17274	-
8M + NH ₄ -8H ₂ O ⁺	C ₅₆ H ₃₆ NO ₂₄ ⁺	1106.16222	1106.16187	0.51
9M + NH ₄ -7H ₂ O ⁺	C ₆₃ H ₄₄ NO ₂₉ ⁺	1278.19940	1278.19873	1.02
9M + NH₄-8H₂O⁺	C₆₃H₄₂NO₂₈⁺	1260.18879	1260.18896	0.25
9M + NH ₄ -9H ₂ O ⁺	C ₆₃ H ₄₀ NO ₂₇ ⁺	1242.17822	1242.17822	0.69
10M + NH₄-9H₂O⁺	C₇₀H₄₆NO₃₁⁺	1396.20483	1396.20557	0.40
10M + NH ₄ -10H ₂ O ⁺	C ₇₀ H ₄₄ NO ₃₀ ⁺	1378.19427	1378.19531	0.88

Note. Bold letters indicate abundant ion species. Clusters marked with * were used for internal calibration. RMSE, root mean square mass error.

TABLE 2 Overview of all identified DHB ions belonging to the $[aM + \text{NH}_4 - b\text{H}_2\text{O}]^+$ ($a = 1, 2, 3, \dots; b \leq a$) series detected on tissue in **positive** ion mode

Figure S3 [supporting information]). MS/MS data of selected 2,5-DHB clusters from each cluster series are included in Figures S18–S23 (supporting information).

Among the matrices covered in this work, DHB delivers the highest number of matrix ions in both polarities. Furthermore, these ions are periodically distributed over a wide mass range from m/z 100 to around m/z 1400, making DHB ideal for internal and external mass calibration. In this regard, DHB may even be considered as a lower mass analogue of Ultramark 1621.

3.2 | Alpha-cyano-4-hydroxycinnamic acid, sinapic acid, and caffeic acid (CHCA)

The derivatives of cinnamic acid, represented in this study by alpha-cyano-4-hydroxycinnamic acid (CHCA, C₁₀H₇NO₃, 189.04260 u), sinapic acid (SA, C₁₁H₁₂O₅, 224.06847 u), and caffeic acid (CA, C₉H₈O₄, 180.04226 u), are a major class of matrix substances used in the positive ion mode for the analysis of small molecules,²⁸ peptides, and proteins.²⁹ All three matrices exhibited a high affinity toward alkali metal cations and formed a large number of cluster ions. Clusters of CA are detected between m/z 100 and 800 and CHCA clusters between m/z 100 and 900. SA delivers the heaviest clusters, which are detected between m/z 100 and 1500. The majority of the observed ions are formed based on a hydrogen/alkali metal cation

exchange leading to a general sum formula of $[aM + b\text{Alkali}-(b-1)\text{H}]^+$ ($a = 1, 2, 3, \dots; b = 1, 2, 3, \dots$). Often these ions are accompanied by additional ions formed by the loss of water or CO₂ from the cluster body leading to a general sum formula of $[aM + b\text{Alkali}-(b-1)\text{H}-\text{H}_2\text{O}]^+$ and $[aM + b\text{Alkali}-(b-1)\text{H}-\text{CO}_2]^+$. In general, CHCA, SA, and CA clusters containing predominantly K⁺ as charge carriers show a higher abundance than clusters containing predominantly Na⁺ as charge carriers. See Tables S6–S8 (supporting information) for the cluster lists of CHCA, SA, and CA and Figures S4–S6 (supporting information) for single pixel mass spectra on mouse brain tissue.

Similar to DHB, the derivatives of cinnamic acid deliver a large number of abundant signals at high and low mass ranges, making them also ideal for use in internal and external mass calibration in the positive mode.

3.3 | 2[(2E)-3-(4-tert-Butylphenyl)-2-methylprop-2-enylidene]malononitrile (DCTB)

Although primarily used for the positive mode analysis of polymers³⁰ and large unpolar macromolecules³¹ in regular MALDI, 2[(2E)-3-(4-tert-butylphenyl)-2-methylprop-2-enylidene]malononitrile (DCTB, C₁₇H₁₈N₂, 250.14699 u) was shown to be suitable for MALDI MS imaging, particularly for detecting small organic molecules.^{32,33} Characteristically, DCTB ions exhibit the loss of alkyl moieties from

TABLE 3 Overview of the general composition of clusters generated by the matrices investigated in this work

Matrix	General cluster composition in positive ion mode	General cluster composition in negative ion mode
DHB	$[aM + X-bH_2O]^+$ $(X = H^+, NH_4^+, Na^+, K^+; a = 1, 2, 3, \dots; b \leq a)$ $[aM + bAlkali-(b-1)H-cH_2O]^+$ $(a = 1, 2, 3, \dots; b = 1, 2, 3, \dots; c = 0, 1, 2, 3, \dots)$	$[aM-bH + (b-1)Alkali-cH_2O]^-$ $[aM-bH-H + (b-1)Alkali]^-$ $(a = 1, 2, 3, \dots; b = 1, 2, 3, \dots; c = 1, 2, 3, \dots)$
CHCA, SA, CA	$[aM + bAlkali-(b-1)H]^+$ $[aM + bAlkali-(b-1)H-CO_2]^+$ $[aM + bAlkali-(b-1)H-CO_2]^+$ $(a = 1, 2, 3, \dots; b = 1, 2, 3, \dots)$	-
DCTB	$[aM + X-Alkyl]^{+/+}$ $a = 1, 2, 3, \dots; X = H^+, Na^+, K^+;$ $alkyl = CH_4, CH_3, CH_2, C_2H_4, C_2H_6, C_4H_8$	-
pNA	$[aM + X-bNO]^{+/+}$ $(X = H^+, Na^+, K^+; a = 1, 2, 3, \dots; b \leq a)$	$[aM-H-bH_2]^-$ $(a = 1, 2, 3, \dots; b = 1, 2, 3, \dots)$
1,5-DAN	No general cluster composition applicable	$[aM-H-bH_2]^-$ $(a = 1, 2, 3, \dots; b = 1, 2, 3, \dots)$
2,6-DHAP	$[aM + bAlkali-(b-1)H]^+$ $(a = 1, 2, 3, \dots; b = 1, 2, 3, \dots)$	$[aM-H-bH_2]^-$ $[aM-bH + (b-1)Alkali]^-$ $(a = 1, 2, 3, \dots; b = 1, 2, 3, \dots)$
Norharmene	$[aM + X]^+$ $(a = 1, 2, 3, \dots; X = H^+, Na^+, K^+)$	$[aM-H-bH_2]^-$ $(a = 1, 2, 3, \dots; b = 1, 2, 3, \dots)$
THAP	-	$[aM-H-bH_2]^-$ $[aM-bH + (b-1)Alkali]^-$ $(a = 1, 2, 3, \dots; b = 1, 2, 3, \dots)$
9AA	-	$[aM-H-bH_2]^-$ $(a = 1, 2, 3, \dots; b = 1, 2, 3, \dots)$

Note. CA, caffeic acid; CHCA, alpha-cyano-4-hydroxycinnamic acid; 1,5-DAN, 1,5-diaminonaphthalene; DCTB, 2[(2E)-3-(4-tert-butylphenyl)-2-methylprop-2-enylidene]malononitrile; DHAP, 2,6-dihydroxyacetophenone; DHB, 2,5-dihydroxybenzoic acid; 9AA, 9-aminoacridine; pNA, 4-nitroaniline; SA, sinapic acid; THAP, 2,4,6-trihydroxyacetophenone.

the *tert*-butyl group and contain no more than two DCTB base molecules with a single charge carrier that can be H^+ , Na^+ , or K^+ . As a result, DCTB ions were not detected above m/z 550. This leads to a general cluster composition of $[aM + X-Alkyl]^{+/+}$ ($a = 1, 2, 3, \dots; X = H^+, Na^+, K^+; Alkyl = CH_4, CH_3, CH_2, C_2H_4, C_2H_6, C_4H_8$) (Table S9 and Figure S7 [supporting information]).

3.4 | 4-nitroaniline (pNA)

A number of matrix substances are usable in positive and negative ion mode, which significantly increases their utility as general-purpose matrices and makes them suitable for dual polarity measurements. 4-Nitroaniline (pNA, $C_6H_6N_2O_2$, 138.04293 u) is suited for lipid analysis in both ion modes.^{14,34} However, pNA is not vacuum stable and therefore limited to use in intermediate and atmospheric pressure ion sources. As with most matrices usable in the negative ion mode, the clusters of pNA show the loss of molecular hydrogen leading to a general cluster composition of $[aM-H-bH_2]^-$ ($a = 1, 2, 3, \dots; b = 1, 2, 3, \dots$). However, emanating from its nitro-group, pNA forms a

number of clusters with unusual cluster compositions that show the loss of single oxygen atoms, the formal loss of atomic nitrogen via an NO_2/O_2 exchange,³⁵ and the release of nitric oxide (NO). Similar to DCTB, identified clusters of pNA did not exceed the m/z 550 threshold in positive and negative ion mode (Tables S10 and S11 and Figures S8 and S9 [supporting information]). In comparison to other matrices used exclusively in the positive ion mode, pNA generates only a small number of identifiable ions in the positive ion mode, which show a loss of NO. These ions can be described as $[aM + X-bNO]^{+/+}$ ($X = H^+, Na^+, K^+; a = 1, 2, 3, \dots; b \leq a$) (Table S11 and Figure S9 [supporting information]).

3.5 | 1,5-Diaminonaphthalene (1,5-DAN)

In the negative ion mode spectrum of 1,5-diaminonaphthalene (1,5-DAN, $C_{10}H_{10}N_2$, 158.08440 u), which is suitable for the analysis of small molecules and lipids,^{36,37} only a small number of matrix clusters can be assigned unambiguously. All of these clusters are of the $[aM-H-bH_2]^-$ ($a = 1, 2, 3, \dots; b = 1, 2, 3, \dots$) cluster composition

and do not exceed m/z 400 (Table S12 and Figure S10 [supporting information]). Similarly, all 1,5-DAN ions identified in the positive ion mode are found below m/z 400 and do not contain more than two base molecules. In comparison to other positive mode matrices however, 1,5-DAN does not form a protonated molecule. Instead, it forms a highly abundant M^{++} molecular ion (Table S13 and Figure S11 [supporting information]).

3.6 | 2,6-Dihydroxyacetophenone (2,6-DHAP)

2,6-Dihydroxyacetophenone (2,6-DHAP, $C_8H_8O_3$, 152.04734 u), which has been used for the analysis of phospholipids in mouse lung sections,³⁸ forms a small number of cluster ions in negative ion mode of the $[aM-H-bH_2]^-$ ($a = 1, 2, 3, \dots; b = 1, 2, 3, \dots$) and $[aM-bH + (b-1)Alkali]^-$ cluster composition which are detected up to m/z 600. In the positive ion mode, a number of $[aM + bAlkali-(b-1)H]^+$ ions are detected up to m/z 400 (Tables S14 and S15 and Figures S12 and S13 [supporting information]).

3.7 | Norharmane

Beta-carboline, commonly referred to as norharmane ($C_{11}H_8N_2$, 168.06875 u), is a nitrogen-containing heterocycle used for the analysis of lipids in both polarities³⁹ as well as bile acids in the negative ion mode.⁴⁰ In the negative ion mode, identified clusters do not exceed m/z 670 and are mainly of the $[aM-H-bH_2]^-$ ($a = 1, 2, 3, \dots; b = 1, 2, 3, \dots$) cluster composition (Table S16 and Figure S14 [supporting information]). In the positive mode, norharmane forms only a small number of clusters, which are detected up to m/z 540 (Table S17 and Figure S15 [supporting information]). In comparison to other dual polarity mode and positive mode matrices, the ions of norharmane do not show a hydrogen alkali metal cation exchange. These ions contain only a single charge carrier and share the cluster composition $[aM + X]^+$ ($a = 1, 2, 3, \dots; X = H^+, Na^+, K^+$).

3.8 | 2,4,6-Trihydroxyacetophenone (THAP)

2,4,6-Trihydroxyacetophenone (THAP, $C_8H_8O_4$, 168.04225 u) is suited for the negative mode analysis of lipids and small molecules.⁴¹ It mainly forms clusters of the $[aM-H-bH_2]^-$ and $[aM-bH + (b-1)Alkali]^-$ ($a = 1, 2, 3, \dots; b = 1, 2, 3, \dots$) cluster composition up to m/z 540 (Table S18 and Figure S16 [supporting information]).

3.9 | 9-Aminoacridine (9AA)

Similar to norharmane, 9-aminoacridine (9AA, $C_{13}N_{10}N_2$, 194.08440 u) is a nitrogen-containing heterocycle ideal for negative mode analysis of lipids.⁴² 9AA forms only a small number of the clusters of the $[aM-H-bH_2]^-$ ($a = 1, 2, 3, \dots; b = 1, 2, 3, \dots$) cluster composition, which are detected up to m/z 580 (Table S19 and Figure S17 [supporting information]).

4 | MATRIX IONS FOR INTERNAL MASS CALIBRATION IN DRUG AND LIPID IMAGING

A section of murine lung dosed orally with the anti-tuberculosis drug ethambutol (EMB, 100 mg/kg) was imaged using DHB matrix. Highlighted in the hematoxylin and eosin staining of the measured section, which is given in Figure 1A, are the airways and blood vessels present in the section. The measurement was conducted using alternating high mass (m/z 700–900) and low mass (m/z 120–450) full-scan mass windows.²² For internal mass calibration, $[DHB + H-H_2O]^+$ ($C_7H_5O_3^+$) m/z 137.02332 was used in the low mass window and $[5DHB + NH_4-H_2O]^+$ ($C_{35}H_{26}NO_{16}^+$) m/z 716.12461 was used in the high mass window. Figure 1B shows the distribution of the matrix cluster $[2DHB + H-2H_2O]^+$ ($C_{14}H_9O_6^+$) detected at m/z 273.03936 with a root mean square mass error (RMSE) of 0.34 ppm across 23 198 spectra. Due to ion suppression effects, the cluster shows a lower intensity on the tissue. It is known that the mass accuracy of the orbital trapping

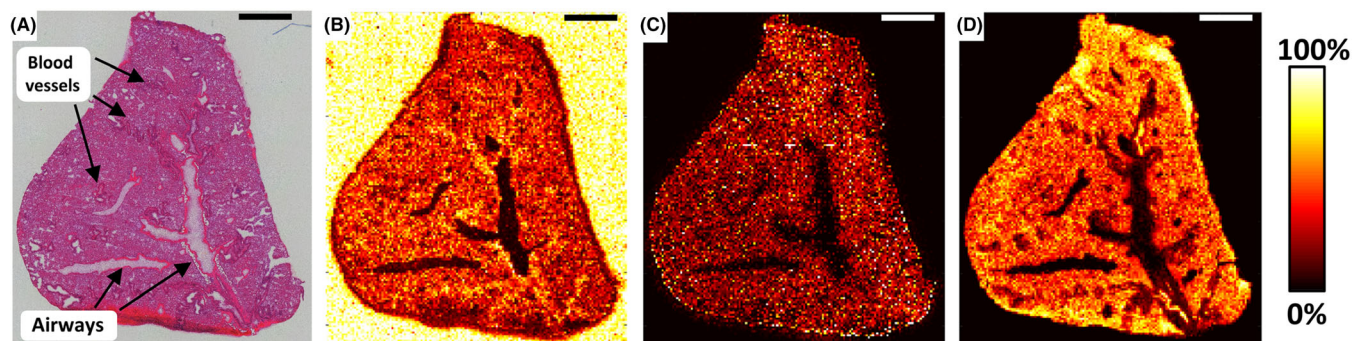


FIGURE 1 MALDI imaging of murine lung section using DHB matrix clusters for internal mass calibration. A) Post measurement haematoxylin and eosin stain. B) Distribution of the DHB cluster $[2DHB + H - 2H_2O]^+$ ($C_{14}H_9O_6^+$) m/z 273.03936. C) Distribution of ethambutol $[M + H]^+$ ($C_{10}H_{25}N_2O_2^+$) m/z 205.19105. D) Distribution of PC 32:0 $[M + K]^+$ ($C_{40}H_{80}NO_8PK^+$) m/z 772.52531. The measurement was carried out in positive ion mode with a raster size of 290×160 pixels and step size of $20 \times 40 \mu m$ resulting in an image pixel size of $40 \times 40 \mu m$

mass analyzers decreases at the edges of the dynamic range.⁴³ Therefore, when choosing a matrix cluster for use in internal mass calibration with this type of instrument, one must consider not only the sample coverage and overall intensity of the cluster but also the intensity ratio between the cluster and the analyte. As expected for orally and intravenously administered drugs, EMB is distributed homogeneously in the lung parenchyma and blood vessels but not inside the airway areas (Figure 1C). The protonated molecule of EMB ($C_{10}H_{25}N_2O_2^+$) is detected at m/z 205.19105 with an RMSE of 0.62 ppm across 14 215 spectra. Figure 1D shows the distribution of the potassiumated molecule of phosphatidylcholine (PC) 32:0 ($C_{40}H_{80}NO_8PK^+$, m/z 772.52531) detected in the high mass window from m/z 700 to 900. In comparison to EMB, PC32:0 is detected only in the lung parenchyma with an RMSE of 0.66 ppm over 15 638 spectra.

5 | CONCLUSION

Matrix ions are ubiquitous in all MALDI MS spectra, therefore providing the ideal internal standard for mass calibration “free of charge” without the need for additional standard substances and sample preparation steps. In many cases, cluster series span a wide mass range. Using the matrix ions identified in this study for mass calibration in combination with high mass resolution can therefore bring about sub-ppm mass accuracy, enabling the identification of targeted compounds, for example, drug compounds directly from an imaging data set, as shown earlier and in our recent work.^{14,22} Matrices used primarily in the positive ion mode tend to generate more matrix ions with higher abundances than matrices designated for use in the negative ion mode. Furthermore, ions generated by positive mode matrices, that is, DHB or cinnamic acid derivatives, tend to cover a wider mass range and are capable of forming heavy clusters with excess of m/z 1500 containing more than 10 base molecules, whereas ions of basic negative mode matrices are typically not detected above m/z 600. The commonality of negative mode matrices is the formation of clusters based on deprotonation followed by the additional loss of hydrogen. This results in little variation in cluster composition between different matrix substances, which simplifies the adaptation of a new matrix substance. Positive mode matrices can be quite different in terms of cluster composition, as can be observed when comparing DHB and CHCA. Whereas DHB clusters are dehydrated and contain a single charge carrier, clusters of cinnamic acid derivatives are usually not dehydrated and show a hydrogen/alkali metal cation exchange, thus containing multiple charge carriers.

ACKNOWLEDGMENTS

The authors thank Kerstin Walter and Christoph Hölscher (FZ Borstel) for providing mouse lung tissue. This work was supported by the Deutsche Forschungsgemeinschaft (INST 91/373-1-FUGG and SFB 1357). Open Access funding enabled and organized by Projekt DEAL.

PEER REVIEW

The peer review history for this article is available at <https://publons.com/publon/10.1002/rcm.9110>.

DATA AVAILABILITY STATEMENT

Data available in article supplementary material.

ORCID

Axel Treu  <https://orcid.org/0000-0002-0999-6241>

Andreas Römpp  <https://orcid.org/0000-0001-8384-9250>

REFERENCES

- Römpp A, Spengler B. Mass spectrometry imaging with high resolution in mass and space. *Histochem Cell Biol.* 2013;139(6):759-783.
- Spengler B. Mass spectrometry imaging of biomolecular information. *Anal Chem.* 2015;87(1):64-82.
- Claude E, Jones EA, Pringle SD. DESI Mass Spectrometry Imaging (MSI). In: Cole LM, ed. *Imaging Mass Spectrometry: Methods and Protocols.* New York, NY: Springer New York; 2017:65-75.
- Agüi-Gonzalez P, Jähne S, Phan NTN. SIMS imaging in neurobiology and cell biology. *J Anal at Spectrom.* 2019;34(7):1355-1368.
- Nilsson A, Goodwin RJA, Shariatgorji M, Vallianatou T, Webbhorn PJH, André PE. Mass spectrometry imaging in drug development. *Anal Chem.* 2015;87(3):1437-1455.
- Gross JH. MALDI Matrices. In: *Mass Spectrometry A Textbook.* 2nd ed. Heidelberg: Springer; 2011:516-527.
- Zenobi R, Knochenmuss R. Ion formation in MALDI mass spectrometry. *Mass Spectrom Rev.* 1999;17(5):337-366.
- Mohan KR, Bartlett MG, Busch KL, Schoen AE, Gore N. Calibration point for electron ionization MS/MS spectra measured with multiquadrupole mass spectrometers. *J Am Soc Mass Spectrom.* 1994;5(6):576-582.
- Jiang L, Moini M. Ultramark 1621 as a reference compound for positive and negative ion fast-atom bombardment high-resolution mass spectrometry. *J Am Soc Mass Spectrom.* 1992;3(8):842-846.
- Kolarova L, Prokes L, Kucera L, et al. Clusters of monoisotopic elements for calibration in (TOF) mass spectrometry. *J Am Soc Mass Spectrom.* 2017;28(3):419-427.
- Lou X, van Dongen JL, Meijer EW. Generation of CsI cluster ions for mass calibration in matrix-assisted laser desorption/ionization mass spectrometry. *J Am Soc Mass Spectrom.* 2010;21(7):1223-1226.
- Kim JW, Ramaswamy BR, Chang KH, Isobe T, Tanabe S. Multiresidue analytical method for the determination of antimicrobials, preservatives, benzotriazole UV stabilizers, flame retardants and plasticizers in fish using ultra high performance liquid chromatography coupled with tandem mass spectrometry. *J Chromatogr a.* 2011;1218(22):3511-3520.
- Guenther S, Römpp A, Kummer W, Spengler B. AP-MALDI imaging of neuropeptides in mouse pituitary gland with 5 μ m spatial resolution and high mass accuracy. *Int J Mass Spectrom.* 2011;305(2):228-237.
- Desbenoit N, Walch A, Spengler B, Brunelle A, Römpp A. Correlative mass spectrometry imaging, applying time-of-flight secondary ion mass spectrometry and atmospheric pressure matrix-assisted laser desorption/ionization to a single tissue section. *Rapid Commun Mass Spectrom.* 2017;32(2):159-166.
- Heiles S, Kompauer M, Müller MA, Spengler B. Atmospheric-pressure MALDI mass spectrometry imaging at 213 nm laser wavelength. *J Am Soc Mass Spectrom.* 2020;31(2):326-335.
- Römpp A, Guenther S, Schober Y, et al. Histology by mass spectrometry: Label-free tissue characterization obtained from high-

- accuracy bioanalytical imaging. *Angew Chem Int Ed*. 2010;49(22):3834-3838.
17. Guo Z, He L. A binary matrix for background suppression in MALDI-MS of small molecules. *Anal Bioanal Chem*. 2007;387(5):1939-1944.
 18. Smirnov IP, Zhu X, Taylor T, et al. Suppression of α -Cyano-4-hydroxycinnamic acid matrix clusters and reduction of chemical noise in MALDI-TOF mass spectrometry. *Anal Chem*. 2004;76(10):2958-2965.
 19. Marijana Petkovic JS, Müller M, Süß R, Arnold K, Arnhold J. Detection of adducts with matrix clusters in the positive and negative ion mode MALDI-TOF mass spectra of phospholipids. *Z Naturforsch*. 2009;64b:331-334.
 20. Moench PA, Catoire A, Glick J, Flarakos J. Determination of tissue-specific ion suppression by liquid extraction surface analysis mass spectrometry. *Rapid Commun Mass Spectrom*. 2015;30(2):340-342.
 21. Taylor AJ, Dexter A, Bunch J. Exploring ion suppression in mass spectrometry imaging of a heterogeneous tissue. *Anal Chem*. 2018;90(9):5637-5645.
 22. Treu A, Kokesch-Himmelreich J, Walter K, Holscher C, Rompp A. Integrating high-resolution MALDI imaging into the development pipeline of anti-tuberculosis drugs. *J Am Soc Mass Spectrom*. 2020;31(11):2277-2286.
 23. Koestler M, Kirsch D, Hester A, Leisner A, Guenther S, Spengler B. A high-resolution scanning microprobe matrix-assisted laser desorption/ionization ion source for imaging analysis on an ion trap/Fourier transform ion cyclotron resonance mass spectrometer. *Rapid Commun Mass Spectrom*. 2008;22(20):3275-3285.
 24. CIAAW. *Current Atomic Masses 2017*; <http://www.ciaaw.org/atomic-masses.htm>. Accessed 10.02, 2019.
 25. Römpp A, Guenther S, Takats Z, Spengler B. Mass spectrometry imaging with high resolution in mass and space (HR2 MSI) for reliable investigation of drug compound distributions on the cellular level. *Anal Bioanal Chem*. 2011;401(1):65-73.
 26. Huber K, Khamahgir-Silz P, Schramm T, Gorshkov V, Spengler B, Rompp A. Approaching cellular resolution and reliable identification in mass spectrometry imaging of tryptic peptides. *Anal Bioanal Chem*. 2018;410(23):5825-5837.
 27. Schiller J, Suss R, Fuchs B, et al. The suitability of different DHB isomers as matrices for the MALDI-TOF MS analysis of phospholipids: Which isomer for what purpose? *Eur Biophys J*. 2007;36(4-5):517-527.
 28. Calvano CD, Monopoli A, Cataldi TRI, Palmisano F. MALDI matrices for low molecular weight compounds: An endless story? *Anal Bioanal Chem*. 2018;410(17):4015-4038.
 29. Angel PM, Caprioli RM. Matrix-assisted laser desorption ionization imaging mass spectrometry: In situ molecular mapping. *Biochemistry*. 2013;52(22):3818-3828. <https://doi.org/10.1021/bi301519p>
 30. Winter JD, Deshayes G, Boon F, Coulembier O, Dubois P, Gerbaux P. MALDI-ToF analysis of polythiophene: Use of trans-2-[3-(4-t-butylphenyl)-2-methyl-2-propenylidene]malononitrile—DCTB—As matrix. *J Mass Spectrom*. 2011;46(3):237-246.
 31. Wyatt MF, Stein BK, Brenton AG. Characterization of various Analytes using matrix-assisted laser desorption/ionization time-of-flight mass spectrometry and 2-[(2E)-3-(4-tert-Butylphenyl)-2-methylprop-2-enylidene]malononitrile matrix. *Anal Chem*. 2006;78(1):199-206.
 32. Peukert M, Matros A, Lattanzio G, Kaspar S, Abadía J, Mock H-P. Spatially resolved analysis of small molecules by matrix-assisted laser desorption/ionization mass spectrometry imaging (MALDI-MSI). *New Phytol*. 2011;193(3):806-815.
 33. Rzagalinski I, Kovačević B, Hainz N, Meier C, Tschernig T, Volmer DA. Toward higher sensitivity in quantitative MALDI imaging mass spectrometry of CNS drugs using a nonpolar matrix. *Anal Chem*. 2018;90(21):12592-12600.
 34. Steven RT, Race AM, Bunch J. Para-Nitroaniline is a promising matrix for MALDI-MS imaging on intermediate pressure MS systems. *J Am Soc Mass Spectrom*. 2013;24(5):801-804.
 35. Treu A, Rittner M, Kemken D, Schiebel H-M, Spitteller P, Dülcks T. Loss of atomic nitrogen from even-electron ions? A study on benzodiazepines. *J Mass Spectrom*. 2015;50(8):978-986.
 36. Korte AR, Lee YJ. MALDI-MS analysis and imaging of small molecule metabolites with 1,5-diaminonaphthalene (DAN). *J Mass Spectrom*. 2014;49(8):737-741.
 37. Dueñas ME, Carlucci L, Lee YJ. Matrix recrystallization for MALDI-MS imaging of maize lipids at high-spatial resolution. *J Am Soc Mass Spectrom*. 2016;27(9):1575-1578.
 38. Berry KAZ, Li B, Reynolds SD, et al. MALDI imaging MS of phospholipids in the mouse lung. *J Lipid Res*. 2011;52(8):1551-1560.
 39. Scott AJ, Flinders B, Cappell J, et al. Norharmaline matrix enhances detection of endotoxin by MALDI-MS for simultaneous profiling of pathogen, host, and vector systems. *Pathog Dis*. 2016;74(8). <https://doi.org/10.1093/femspd/ftw097>
 40. Genangeli M, Heijens AMM, Rustichelli A, et al. MALDI-mass spectrometry imaging to investigate lipid and bile acid modifications caused by lentil extract used as a potential Hypocholesterolemic treatment. *J Am Soc Mass Spectrom*. 2019;30(10):2041-2050.
 41. Prentice BM, Chumbley CW, Caprioli RM. High-speed MALDI MS/MS imaging mass spectrometry using continuous raster sampling. *Journal of Mass Spectrometry: JMS*. 2015;50(4):703-710.
 42. Cerruti CD, Benabdellah F, Laprévotte O, Touboul D, Brunelle A. MALDI imaging and structural analysis of rat brain lipid negative ions with 9-Aminoacridine matrix. *Anal Chem*. 2012;84(5):2164-2171.
 43. Makarov A, Denisov E, Lange O, Horning S. Dynamic range of mass accuracy in LTQ Orbitrap hybrid mass spectrometer. *J Am Soc Mass Spectrom*. 2006;17(7):977-982.

SUPPORTING INFORMATION

Additional supporting information may be found online in the Supporting Information section at the end of this article.

How to cite this article: Treu A, Römpp A. Matrix ions as internal standard for high mass accuracy matrix-assisted laser desorption/ionization mass spectrometry imaging. *Rapid Commun Mass Spectrom*. 2021;35(16):e9110. <https://doi.org/10.1002/rcm.9110>